Validation of the actuator line method for simulating flow through a horizontal axis tidal stream turbine by comparison with measurements

Mohammad H. Baba-Ahmadi*

School of Engineering, Physics and Mathematics, University of Dundee, Dundee, DD1 4HN, UK

Ping Dong

School of Engineering, The Quadrangle, The University of Liverpool, Brownlow Hill, Liverpool, L69 3GH, UK

Abstract

The purpose of the present work is to evaluate the capability of the Actuator Line Method (ALM) to simulate flow through a horizontal axis tidal stream turbine. A numerical model combining the ALM with large eddy simulation technique is developed and applied to compute the flow past a laboratory-scale tidal stream turbine. The flow field is analysed in terms of streamwise mean velocity, turbulence intensity, turbulent kinetic energy and the decay rate of the maximum turbulent kinetic energy behind the turbine. It is found that the ALM performs well in predicting the mean flow and turbulence characteristics behind the turbine. The flow field predicted show a clear transition from an organised vorticity region near the turbine to a highly turbulent flow downstream. The location of this transition and the controlling parameters are discussed but further investigation, both numerical and experimental is required in order to clarify its effects on the flow structure and the performance of downstream turbines in tidal turbine arrays.

Keywords: Tidal stream turbine, Actuator line method, Large eddy simulation

1. INTRODUCTION

The interest in tidal stream energy worldwide is driven by three aspects of the resource: it is renewable, predictable (different from wave and wind), and amply available. Despite the considerable research effort in the past decade, the take-up, to date, of the technology remains slow. At the present time, the marine energy industry is lagging behind the wind energy industry. Many scientific and technological hurdles remain to be overcome before the identified potential of marine energy can be fulfilled. In studying Tidal Stream Turbines (TSTs) Computational Fluid Dynamics (CFD) has long played a key role either for better understanding the flow structure around TSTs or designing more efficient TST blades and accurately predicting their performance especially in TST arrays. Quantifying the complicated wake field of TST is identified as important for the design of both isolated TST and TST arrays.

*Corresponding author
Email addresses: m.babaahmadi@dundee.ac.uk (Mohammad H. Baba-Ahmadi), ping.dong@liverpool.ac.uk (Ping Dong)

Nomenclature			
		u'	axial rms velocity component (m/s)
		V_{rel}	relative velocity vector (m/s)
B	number of blades	v_θ	tangential velocity component (m/s)
c	chord length (m)	v_r	radial velocity component (m/s)
C_L, C_D	lift and drag coefficients	α	local angle of attack
$f_{i,\epsilon}$	blade loading (N)	γ	local pitch angle
k	sub-grid kinetic energy (m^2s^{-2})	λ	tip speed ratio ($\Omega R/U$)
p	pressure(N/m^2)	Δ	local grid size (m)
R, D	radius and diameter of turbine (m)	ν	kinematic viscosity (m^2/s)
Re	Reynolds number (UR/ν)	ν_t	SGS eddy viscosity (m^2/s)
Re_c	chord based Reynolds number ($V_{rel}c/\nu$)	ρ	density (kg/m^3)
TKE	turbulent kinetic energy (m^2s^{-2})	τ_{ij}	Reynolds stresses (m^2s^{-2})
U	upstream flow velocity (m/s)	ϕ	incident flow angle
u	axial mean velocity component (m/s)	Ω	angular velocity (s^{-1})

However, vortex modelling of tidal stream turbine wake still poses some serious challenges, especially in the near wake region where the blades trailing vorticity is concentrated in tip and root vortices, subject to important deformation and turbulent diffusion. Among the CFD models applied to study TST hydrodynamics the models solving the Reynolds-averaged NavierStokes (RANS) equations and Large Eddy Simulations (LES) are most widely used. Lawson *et al.* [1], Mason-Jones *et al.* [2] and Jo *et al.* [3] used full RANS model and Kang *et al.* [4], Lloyd *et al.* [5] and Afgan *et al.* [6] used full LES model for their TST simulations. They modelled the true turbine blade geometry with the no-slip condition being applied at turbine blade surface.

In order to increase computational efficiency, various simplified methods have been developed to use distributed volume forces in these CFD models to represent the action of turbine blades. Two notable methods that were originally developed in wind turbine industry are often used to simulate TSTs: the Actuator Disk Method (ADM) and Actuator Line Method (ALM). In these techniques, the loading on the turbine blades is calculated from airfoil data and turbulence is created from the prescribed body forces, thus avoiding the computation of the blade boundary layer flow and reducing significantly the number of computational points required. The computational cost for a LES model for the ambient flow coupled with ADM or ALM representing TST effects is considerably reduced compared with that of the full LES model. For this reason these methods have been widely adopted to simulate either individual TST or TST arrays. For example, Batten *et al.* [7], Gant & Stallard [8] and Nishino & Willden [9] used RANS/ADM to model a single TST and Churchfield *et al.* [10] used LES/ALM to simulate TST arrays. The limited validation tests carried out in the wind turbine field (e.g. Martinez *et al.* [11]) show that the ALM and ADM predict similar wake profiles and power output but the ALM is better at reproducing the vortical structures around individual blades as it is able to resolve the root- and tip-vortices.

The ALM technique, first developed by Sørensen & Shen [12] and later reformulated by Mikkelsen [13],

has already been applied and validated to simulate flows through horizontal axis wind turbines [14, 15]. This method has recently been used to simulate horizontal axis tidal turbines [10] in which the LES and ALM are combined to simulate TST arrays. But to the authors' best knowledge, there is no other published work which applies LES/ALM method to simulate TSTs and compares the predicted results with detailed measurements. In this study the LES/ALM technique is used to simulate a three-bladed laboratory scale TST and the numerical results are compared to experimental data of Tedds *et al.* [16] to validate the method. The aim of the research is to demonstrate the capability and accuracy of the LES/ALM technique in simulating TSTs by examining spatial distribution of flow velocity, turbulence intensity and turbulent kinetic energy.

2. NUMERICAL MODELLING

2.1. LES governing equations

The LES method is used in this study. The larger turbulent scales are directly resolved by solving the spatially filtered Navier-Stokes equations, whereas the effects of the remaining, more isotropic, smaller scales are modelled with a subgrid-scale (SGS) turbulence model. LES provides more flow physics detail and places less reliance on turbulence modelling, than the more computationally efficient RANS type of CFD models, in which all turbulent scales are modelled. Unlike direct numerical simulation (DNS), in which all turbulent scales are resolved, LES remains computationally tractable for high Reynolds numbers flows. Here the turbine blades are not resolved (i.e. a grid is not fitted around the blades). Rather, the actuator lines are used in which the forces created by the turbine blades are modelled and applied to the flow field as a body force.

In LES, the governing equations are obtained by filtering the time-dependent Navier-Stokes equations in physical space, such that those eddies which are below a certain size are filtered out. The resulting equations thus only govern the dynamics of the large scales, although the smaller scales usually are modelled by some eddy-viscosity-based sub-grid scale (SGS) models. The filtered incompressible Navier-Stokes equations in velocity-pressure variables are written as

$$\frac{\partial \bar{u}_i}{\partial x_i} = 0 \tag{1}$$

$$\frac{\partial \bar{u}_i}{\partial t} + \frac{\partial (\bar{u}_i \bar{u}_j)}{\partial x_j} = -\frac{1}{\rho}\frac{\partial \bar{p}}{\partial x_i} + \nu \frac{\partial^2 \bar{u}_i}{\partial x_j^2} + \frac{\partial \tau_{ij}}{\partial x_j} + f_{i,\epsilon} \tag{2}$$

where the bar denotes filtering, and $\bar{u}_j = u_j - u_j^{sgs}$ is the resolved-scale velocity vector, which is the instantaneous velocity vector, u_j, minus the SGS velocity vector, u_j^{sgs} and $f_{i,\epsilon}$ is the body force provided from the actuator line method described in section 2.2.

2.1.1. Subgrid scale model

The resulting SGS Reynolds stresses are modelled with an eddy viscosity as

$$\tau_{ij} = -\nu_t \left(\frac{\partial \bar{u}_i}{\partial x_j} + \frac{\partial \bar{u}_j}{\partial x_i} \right) + \frac{2}{3} k \delta_{ij} \tag{3}$$

Here, the eddy viscosity, ν_t, is determined by solving an extra equation for the subgrid kinetic energy. The subgrid kinetic energy equation can be modelled as

$$\frac{\partial k}{\partial t} + \bar{u}_j \frac{\partial k}{\partial x_j} = \frac{\partial}{\partial x_j}\left(\frac{\nu_t}{\sigma_k}\frac{\partial k}{\partial x_j}\right) - \tau_{ij}\frac{\partial \bar{u}_i}{\partial x_j} - \epsilon_k \tag{4}$$

where

$$\epsilon_k = C_\epsilon \frac{k^{3/2}}{\Delta} \qquad , \qquad \nu_t = C_k k^{1/2} \Delta \tag{5}$$

and σ_k, C_k and C_ϵ are model coefficients introduced in [17] and Δ is the local cell size.

2.2. Turbine modelling

In LES, turbulence is originally generated in the wall boundary layer by resolving it on a fine mesh. This requires very small cell sizes and time steps, and makes LES very expensive when Reynolds numbers are high. To prevail over this problem, in this study the geometry of the turbine is not resolved and instead, the turbine is represented using a method developed by Sørensen & Shen [12]. Using this method, by avoiding the requirement to solve the boundary layer in detail, the applied forces on the rotor blades are calculated from airfoil data. With ignoring the blade geometry, turbulence will be generated from the movement of the body forces and the interaction of the moving body forces with the bed boundary layer. The computational cost for LES/ALM computations is somewhat comparable to that of unsteady full RANS computations because LES/ALM avoids resolving the blade boundary layer.

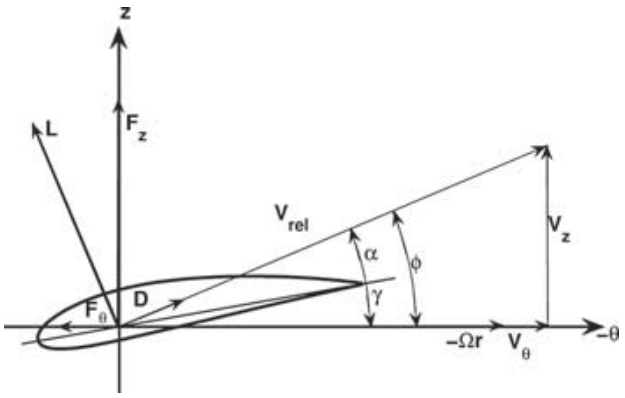

Figure 1: Cross-sectional airfoil element showing velocity and force vectors.

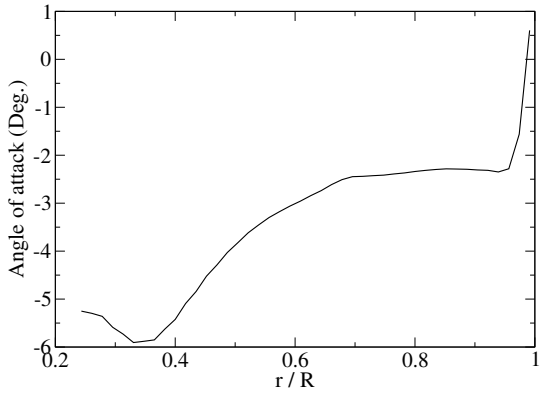

Figure 2: Angle of attack on the actuator lines.

In this technique, a three-dimensional Navier-Stokes solver is coupled with the actuator line method in which body forces are distributed along rotating lines representing the turbine blades. Therefore, full 3D Navier-Stokes simulations predict the flow field and loads on each blade are determined from the local angle of attack and tabulated airfoil data.

Having the flow field together with the blade geometry, a blade element approach combined with tabulated 2D airfoil characteristics is used to determine the loads on the rotor blades. Figure 1 shows a cross-sectional airfoil element at radius r in the (θ, z) plane.

The velocity triangle shown in Figure 1 is used to calculate the local velocity relative to the rotating blade as follows:

$$V_{rel} = \sqrt{\mathrm{v}_z^2 + (\Omega r - \mathrm{v}_\theta)^2} \tag{6}$$

where Ω is the angular velocity and $\mathrm{v_z}$ and v_θ present the axial and tangential velocities, respectively. As shown in Figure 1, the local angle of attack is given by $\alpha = \phi - \gamma$, where γ denotes the local pitch angle and ϕ is the flow angle between $\mathrm{V_{rel}}$ and the rotor plane calculated as:

$$\phi = \tan^{-1}\left(\frac{\mathrm{v}_z}{\Omega r - \mathrm{v}_\theta}\right) \tag{7}$$

The force per spanwise unit length normalised by density can be calculated using the determined angle of attack and relative velocity as:

$$\mathbf{f}_{2D} = \frac{1}{2} c V_{rel}^2 (C_L \mathbf{e}_L + C_D \mathbf{e}_D) \tag{8}$$

here $\mathrm{C_L} = \mathrm{C_L}(\alpha, \mathrm{Re_c})$ and $\mathrm{C_D} = \mathrm{C_D}(\alpha, \mathrm{Re_c})$ present the lift and drag coefficients, respectively, $\mathrm{Re_c}$ is the Reynolds number based on the chord length, c, and $\mathbf{e}_L$ and $\mathbf{e}_D$ are the unit vectors in the lift and the drag directions, respectively.

The airfoil data obtained directly from 2D measurements or computations need to be corrected for rotational effects caused by Coriolis and centrifugal forces, especially for cross sections near the root. Furthermore, airfoil cross sections near the blade tip are influenced by the tip effect caused by the pressure equalization from the pressure and suction sides at the tip. As a consequence, the tip flow is different from the corresponding 2D flow at the same angle of attack. To take into account these effects, a correction factor developed by Shen *et al.* [14] is applied on the calculated 2D forces. The function is

$$F_1 = \frac{2}{\pi} \cos^{-1}\left[\exp\left(-g\frac{B(R-r)}{2r\sin\phi}\right)\right] \tag{9}$$

where B is the number of blades, ϕ is the flow angle and the function g is defined as

$$g = \exp(-0.125(B\Omega R/U_\infty - 21)) + 0.1 \tag{10}$$

On the other hand, to avoid singular behaviour and numerical instability, the modelled blade forces are distributed smoothly on several mesh points along and away from the actuator lines using a 3D Gaussian projection. In practice, the resulting body force, $\mathbf{f}_\epsilon$, is then formed by taking the convolution of the computed force, $\mathbf{f}_{2D}$, correction factor $\mathrm{F_1}$, and a regularization kernel η_ϵ as shown below:

$$\mathbf{f}_\epsilon(\mathbf{x}) = \sum_{i=1}^{B} \int_0^R F_1 \mathbf{f}_{2D}(r) \eta_\epsilon(|\mathbf{x} - r\mathbf{e}_i|) dr \tag{11}$$

where $\mathbf{e}_i$ is the unit vector of the $\imath$th blade direction and $|\mathbf{x} - r\mathbf{e}_i|$ is the distance between cell-centred grid points and points at the $\imath$th actuator line, η_ϵ is the regularization kernel defined as

$$\eta_\epsilon(r) = \frac{1}{\epsilon^3 \pi^{3/2}} \exp\left[-r^2/\epsilon^2\right] \tag{12}$$

and ϵ is a parameter that serves to adjust the concentration of the regularized load and takes a value between 2 and 3 cell sizes, Troldborg [18].

Since there was no experimental airfoil data, C_L and C_D, for the blade used in the experiment, these data were generated numerically using XFOIL. The XFOIL code has been validated against other numerical methods and experimental data at both low and moderate angles of attack. As the numerical results for the angle of attack (AoA) presented in Figure 2 shows, for the simulated experiment, there are $|\text{AoA}| \leq 10^\circ$ and XFOIL outputs should be reliable [19]. To avoid any inconsistency and have a smooth transition for airfoil data between various sections of the blade, 20 sections were generated in radial direction using AutoCAD.

2.3. Flow solver

The filtered incompressible Navier-Stokes equations together with the SGS model are solved using the CFD code library OpenFOAM [20, 21]. This is a C++ code library of classes for writing CFD codes. The governing equations are discretised using the finite volume method. Although the solver is unstructured, the grid used here is composed of hexahedral elements and could be described in a structured way. Integration of the dependent variables over each cell, together with application of Gauss' theorem, generates a set of discretised equations with the divergence terms represented as fluxes across the cell faces, evaluated using an appropriate centred second order interpolation scheme (gamma scheme). Time integration is carried out by the Crank-Nicholson scheme, which is second order in time. Following the procedure of Rhie & Chow [22] a Poisson equation is constructed which implements the incompressibility condition (Eq. 1), and the equation set solved sequentially using the PISO algorithm. Solution is performed implicitly by matrix inversion using Incomplete Cholesky Conjugate Gradient methods.

2.4. Computational domain and boundary conditions

2.4.1. Computational domain set up

In this study, a horizontal axis laboratory scale TST comprising of three blades has been numerically simulated with the hybrid LES/ALM technique. All geometrical and model details conform to the experimental setup of Tedds *et al.* [16]. The experiment was undertaken in the high speed re-circulating water flume at the University of Liverpool. Figure 3 shows schematically the assembled 0.5m diameter, three-bladed configuration of the horizontal axis tidal turbine (HATT) used in the experiment. The water flows into the working section which is 3.7m long by 1.4m wide. The conditions under which the experimental test was made were 0.8 m water depth with the turbine located at a depth of 0.425m. The rotor was run at a tip speed ratio $\lambda = \Omega R/U = 6.15$, a pitch angle 6° and, a water flow with $\text{Re} = UR/\nu = 2.22 \times 10^5$ and a measured turbulence intensity of 2%.

Unsteady computations were carried out using a Cartesian mesh of 2.3×10^6 mesh points in a domain of size $10\text{m} \times 1.2\text{m} \times 0.8\text{m}$ with the finest cell size nearly R/30 in the turbine plane, where R is the rotor radius. From a numerical point of view, a discretization of R/30 has been found sufficient for the LES/ALM simulations, Sørensen & Shen [12] and Shen *et al.* [14]. The rotor centre was located at a section 3m

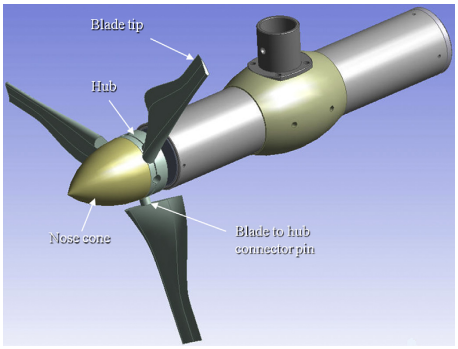

Figure 3: Schematic of the scale HATT.

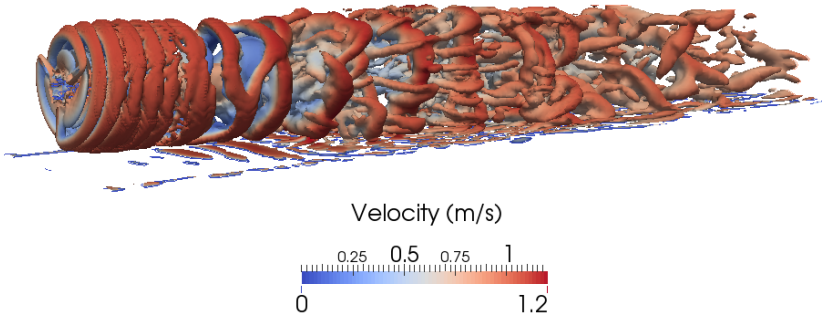

Figure 4: Instantaneous view of the flow field. Isometric view of the second invariant of the velocity gradient tensor coloured by the mean velocity.

downstream of the inlet and a height 0.375 from the bed. The time step is chosen to be 10^{-3}R/U, and due to a highly turbulent flow in the far-wake, each run allows water to get through the channel three times. In this simulation, besides replacing turbine blades with actuator lines, the vertical support is ignored and the nacelle is represented by a short cylinder. To avoid using a very fine mesh and increasing computational cost, the larger scales are not resolved near the bed and the short cylinder modelling the nacelle; instead, a wall model is used. In this simulation, due to lack of the experimental mean velocity profiles, the inlet velocity conditions are generated using the 1/7 power law velocity profile with super-imposing white noise with intensity %2.

2.4.2. Boundary conditions

In this simulation, divergence-free organized perturbations superimposed upon a power law mean velocity profile are used as an upstream boundary condition. On the downstream boundary, the normal gradient of velocity is zero, and the resulting velocity flux through that boundary is adjusted to maintain global continuity. The gradient of pressure normal to the upstream is zero and pressure is fixed on downstream. The side boundaries are set to periodic conditions. The upper boundary is approximated as an impenetrable, no stress lid, instead of simulating a free surface [23, 24]. No slip condition and zero normal gradient for pressure are applied for the bed boundary and the short cylinder modelling the nacelle.

3. RESULTS AND DISCUSSION

The numerical results for streamwise mean velocity, longitudinal turbulence intensity and turbulent kinetic energy are compared to the experimental data disseminated by Tedds *et al.* [16]. As reported in the paper [16], the statistical uncertainty in the mean velocities is estimated to be better than 1%. The quantities are normalised by inflow mean velocity and turbine diameter which are U = 0.9m/s and D = 0.5m respectively. The presented results are for the test case with the tip speed ratio $\lambda = 6.15$. Figure 4 gives an instantaneous view of the flow field behind the turbine and clearly shows a flow regime transition further downstream.

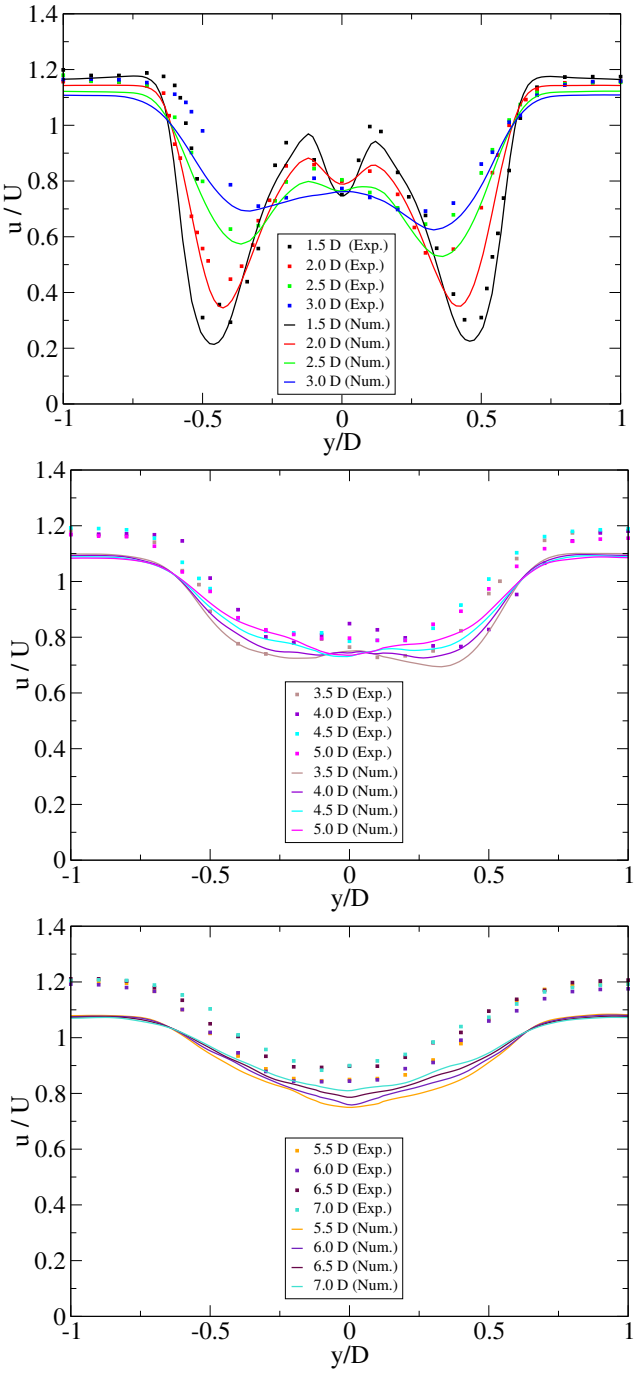

Figure 5: Axial velocity behind the turbine at the rotor axis height.

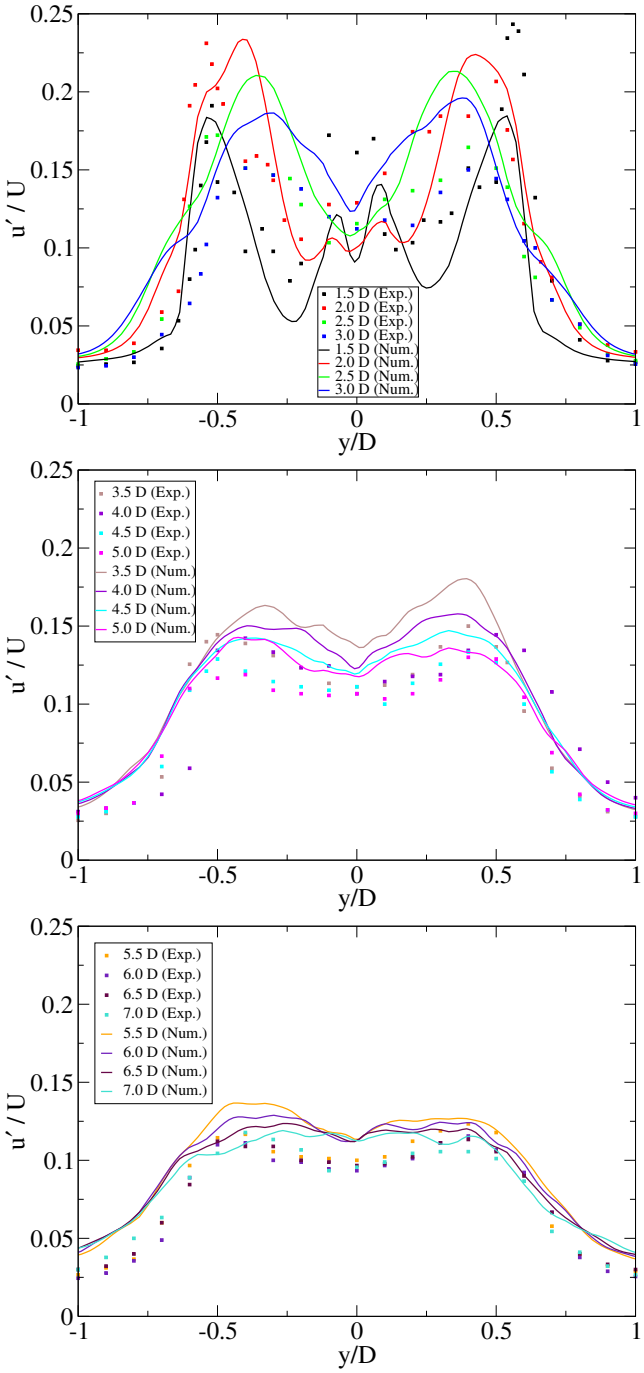

Figure 6: The longitudinal turbulence intensity at the rotor axis height.

Figure 4 presents an isometric view of the second invariant of the velocity-gradient tensor sometimes called the 'Q criterion' coloured by the mean velocity.

3.1. Mean flow

Figure 5 shows the normalised mean streamwise velocities behind the turbine in horizontal planes at the rotational axis height and up to seven diameter distances downstream. Corresponding to the experimental data the first results are presented for a distance 1.5D behind the turbine. In Figure 5 the results for distances 1.5D to 3.0D, 3.5D to 5.0D and 5.5D to 7.0D from the turbine are presented in the top, middle and bottom frames respectively. The results show a good agreement considering the point that the true geometry of the blade has not been modelled in the applied LES/ALM technique. The plots show that the agreement is less good further downstream. There can be some possible reasons such as ignoring the blockage effect [25] by using periodic boundaries at side walls or predicting the transition in the flow with a shift compared to the experiment which leads to a delay in starting wake recovery as explained in the section 3.3, and its well understanding requires further investigations. Also the numerical results at 1.5D and 2.0D downstream are more symmetric in comparison to corresponding experimental data that might be due to the vertical support used in the experiment which is not modelled here for numerical simulation.

3.2. Turbulent flow field

u', v' and w' are defined as the root mean square of velocity components. The longitudinal turbulence intensity, u'/U, in horizontal planes at the rotor axis height are presented in Figure 6. The values are for distances 1.5D to 7.0D from the turbine plane. Like the results for the mean velocity, here the numerical results are more symmetric especially close to turbine due to not modelling the vertical support in the numerical simulation. The plots show a good agreements between computed and experimental results except for the first plot (black line) presenting the points at a distance 1.5D behind the turbine which shows a lower level of u' in comparison to the corresponding experimental data. It can be referred to the flow regime transition behind the turbine as shown in Figure 4. It will be explained in more detail later in the section 3.3 (Figure 10).

Figure 7 shows spanwise distributions of the normalised turbulent kinetic energy (TKE) behind the turbine where TKE differs from the sub-grid kinetic energy and is defined as $\mathrm{TKE} = \frac{1}{2}(u'^2 + v'^2 + w'^2)$. The TKE plots are presented for the same places as those explained in Figures 5 and 6. Plots show a good agreement between CFD and experimental results except for the first plot (solid black line) similar to the first plot for u' in Figure 6 with the same reason considering the above relation for TKE which will be explained later by referring to Figure 10.

3.3. Wake characteristics

The maximum of turbulence intensity at different depths are depicted in Figure 8 and both numerical and experimental results show a decrease in the maximum value further downstream. While for the streamwise component (Figure 8, top frame), the CFD results show a good agreement with the experimental data for all heights with some over predictions further downstream, there are high discrepancies for v' and w' at heights 0.5D below and above the rotor axis for the points up to 4 diameter downstream. Predicting the transition

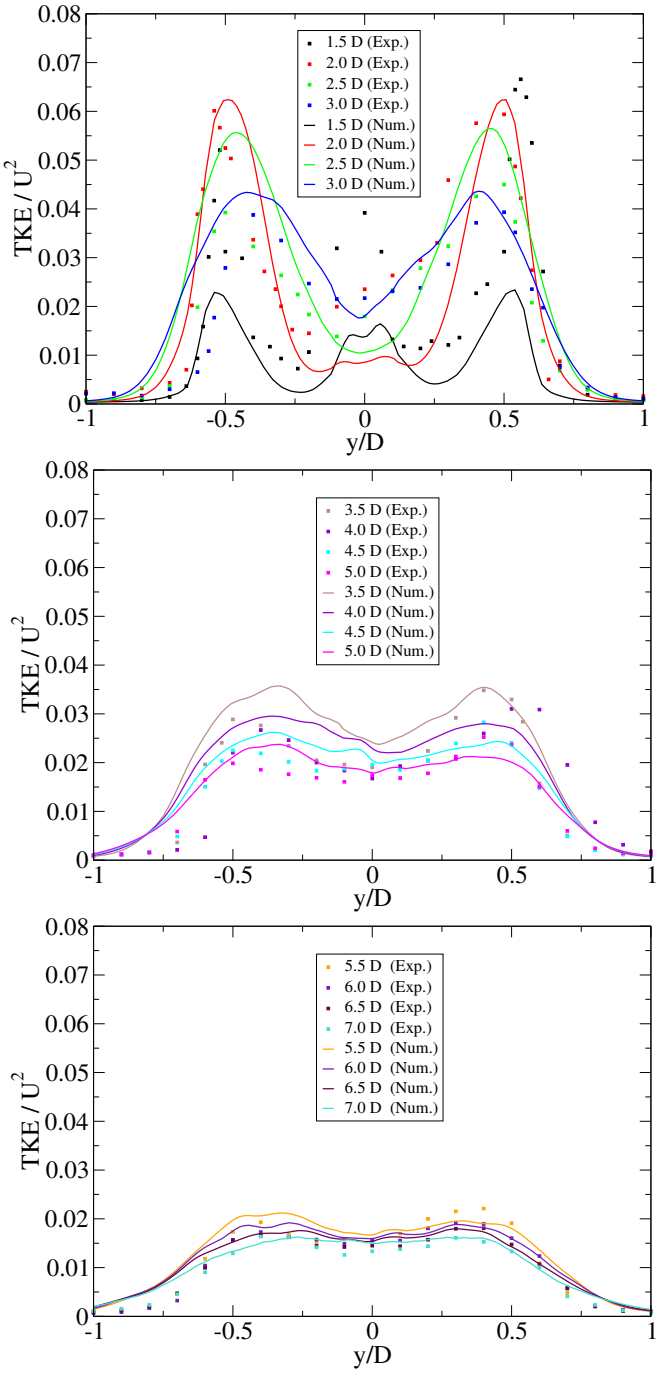

Figure 7: Turbulent kinetic energy behind the turbine at the rotor axis height.

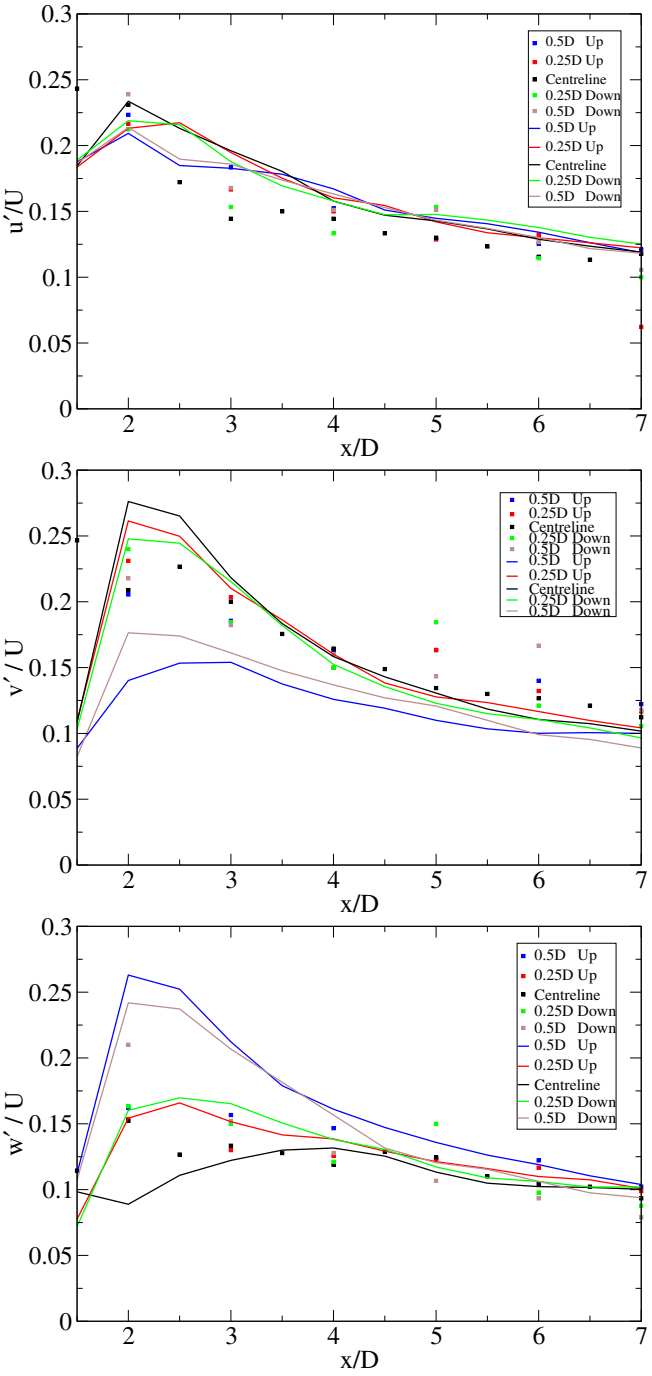

Figure 8: The maximum of turbulence intensity at the various heights downstream; squares: Exp., lines: CFD.

in the domain with a shift compared to the experiment which leads to a delay in starting wake recovery can be considered as a possible reason for the over-estimations appeared in numerical results for u′. But high discrepancies seen for v′ and w′ suggest to examine other reasons such as the effect of turbulence models on numerical results which will be investigated in future work. The numerical results show an interesting point

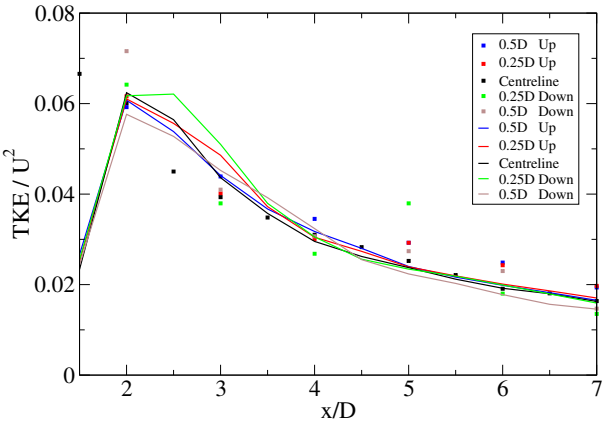

Figure 9: The maximum of the turbulent kinetic energy at the various heights downstream; squares:Exp., solid lines: CFD.

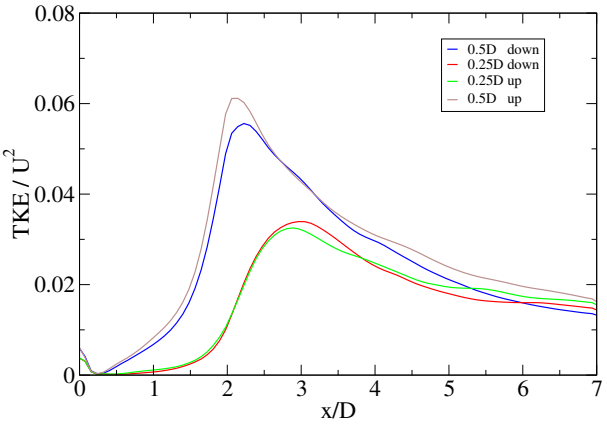

Figure 10: The normalised turbulent kinetic energy at the vertical centre plane at different heights downstream.
.

which is not seen in the experimental data due to absence of data for the distances less than 2D behind the turbine. The numerical results for the u′, v′ and w′ show that there is a peak in the turbulence intensity in the transition zone at 1.5D-2D behind the turbine. The numerical results for TKE shown in Figure 9 also confirm this peak for TKE. Figure 10 gives a better view about the changes of TKE behind the turbine.

Figure 10 shows plots for turbulent kinetic energy on the vertical centre plane at four heights; 0.5D and 0.25D below, and 0.5D and 0.25D above the rotational axis. The plots show two peaks in the streamwise direction for TKE; the first one in the turbine plane and the second one around 1.5D-2D downstream. Figure 4 shows a flow regime transition in the corresponding zone which can be due to the high tip speed ratio ($\lambda = 6.15$) and the reason of the second peak. Considering the plots in Figure 10 and comparing the experimental and numerical plots for the points at 1.5D behind the turbine in Figures 6 and 7, indicates that the predicted place of transition in numerical simulation differs from that in the experiment. While the numerical simulation predicts it happens somewhere about 2D behind the turbine, the experimental data for the points at 1.5D behind the turbine suggest that the transition should be somewhere between 1.5D-2D distances downstream and because of that for these points (1.5D downstream) values of u′ and TKE in the experiment are higher than those in the numerical simulation. Comparing the transition in this test case with the similar transition in general turbulent flows can explain the reason of the mentioned differences in the results. Similar to general turbulent flows, the transition in the flow behind the turbine is sensitive to the upstream conditions. Since in this study, the vertical support is not modelled and the nacelle is represented by a short cylinder and also the inlet velocity profiles are modelled using the 1/7 power law, thus the upstream conditions and, in turn, the predicted transition zone in the numerical simulation would differ from those in the experiment.

4. CONCLUSION

The LES/ALM technique was validated against the detailed laboratory measurements. The model predictions broadly match experimental data for mean velocity, longitudinal turbulence intensity, turbulent kinetic energy and the decay rate of the maximum turbulent kinetic energy behind the turbine. However, a large discrepancy in the rate of maximum spanwise and vertical components of turbulence intensity exists although the sreamwise component is well predicted. The reasons for the discrepancies between numerical results and experimental data can be attributed to the differences in the upstream conditions due to specifying the inflow conditions using the 1/7 power law velocity profile with super-imposed white noise, ignoring vertical support and modelling the nacelle using a short cylinder. It is worth noticing that a transition from vortical flow to turbulent flow behind the turbine is predicted and further studies are under way to determine its structure, the mechanism of its formation and the controlling parameters. Considering the full LES modelling is yet impractical for full scale TST simulation, and the RANS type models or actuator disc method are unable to predict the fine details of the flow structure downstream, the LES/ALM model presented here can serve as a practical numerical technique for tidal stream turbine simulations, especially tidal turbine arrays. Investigating in details the flow structure in near- and far-wakes including tip and hub vortices, transition zone and wake recovery is in progress using the developed code.

Acknowledgements

We would like to thank Prof Rob Poole and his group at the University of Liverpool for providing the blade geometry and experimental data. This work was funded by the Supergen Marine Challenge Programme of the EPSRC (EP/J010359/1).

References

[1] M. J. Lawson, Y. Li, D. C. Sale, Development and verification of a computational fluid dynamics model of a horizontal-axis tidal current turbine, in Proceedings of the 30th International Conference on Ocean, Offshore and Arctic Engineering, Rotterdam, 19th-24th June, 2011.

[2] A. Mason-Jones, D. M. O'Doherty, C.E. Morris, T. O'Doherty, C. B. Byrne, P.W. Prickett, R.I. Grosvenor, I. Owen, S. Tedds, R.J. Poole, Y. X. Wang, Non-dimensional scaling of tidal stream turbines, Energy 44 (1) (2012) 820–829.

[3] C. H. Jo, J. H. Lee, Y. H. Rho, K. H. Lee, Performance analysis of a hat tidal current turbine and wake flow characteristics, Renewable Energy 65 (2014) 175–182.

[4] S. Kang, I. Borazjani, J. A. Colby, F. Sotiropoulos, Numerical simulation of 3d flow past a real-life marine hydrokinetic turbine, Advances in Water Resources 39 (2012) 33–43.

[5] T. P. Lloyd, S. R. Turnock, V. F. Humphrey, Assessing the influence of inflow turbulence on noise and performance of a tidal turbine using large eddy simulations, Renewable Energy 71 (2014) 742–754.

[6] I. Afgan, J. McNaughton, S. Rolfo, D.D. Apsley, P. Stansby, Turbulent flow and loading on a tidal stream turbine by les and rans, International Journal of Heat and Fluid Flow 43 (2013) 96–108.

[7] W. M. J. Batten, M. Harrison, A. S. Bahaj, The accuracy of the actuator disc-rans approach for predicting the performance and far wake of a horizontal axis tidal stream turbine, In: Proc. 9th European Wave and Tidal Energy Conference (EWTEC 2011), 59 September, Southampton, UK.

[8] S. Gant and T. Stallard, *Modelling a Tidal Turbine in Unsteady Flow*, in Proceedings of the Eighteenth International Offshore and Polar Engineering Conference, Vancouver, BC, Canada, July 2008 473–480.

[9] T. Nishino, R. H. J. Willden, Effects of 3-d channel blockage and turbulent wake mixing on the limit of power extraction by tidal turbines, International Journal of Heat and Fluid Flow 37 (2012) 123–135.

[10] M. J. Churchfield, Y. Li, P. J. Moriarty, A large-eddy simulation study of wake propagation and power production in an array of tidal-current turbines, Philosophical Transactions of the Royal Society A 371 (2015) 1–15.

[11] L. A. Martinez, S. Leonardiy, M. J. Churchfield, P. J. Moriarty, A comparison of actuator disk and actuator line wind turbine models and best practices for their use, 50th AIAA Aerospace Sciences Meeting including the New Horizons Forum and Aerospace Exposition 09 - 12 January 2012, Nashville, Tennessee.

[12] J. N. Sørensen, W. Z. Shen, Numerical modelling of wind turbine wakes, Journal of Fluids Engineering 124 (2002) 393–399.

[13] R. Mikkelsen, Actuator Disc Methods Applied to Wind Turbines, Ph.D. Thesis, Technical University of Denmark, Denmark, 2003.

[14] W. Z. Shen, W. J. Zhu, J. N. Sørensen, Actuator line/Navier-Stokes computations for the MEXICO rotor: comparison with detailed measurements, Wind Energy 15(5) (2012) 811–825.

[15] K. Nilsson, W. Z. Shen, J. N. Sørensen, S. P. Breton, S. Ivanell, Validation of the actuator line method using near wake measurements of the MEXICO rotor, Wind Energy 37 (3) (2015) 499–514.

[16] S. C. Tedds, I. Owen, R. J. Poole, Near-wake characteristics of a model horizontal axis tidal stream turbine, Renewable Energy 63 (2014) 222–235.

[17] S. Menon, P. K. Yeung, W. W. Kim, Effect of subgrid models on the computed interscale energy transfer in isotropic turbulence, Computers and Fluids 25(2) (1996) 165–180.

[18] N. Troldborg, Actuator line modeling of wind turbine wakes, Ph.D. Thesis, Department of Fluid Mechanics, Technical University of Denmark, Lyngby, Denmark, 2008.

[19] XFOIL, See https://stuff.mit.edu/afs/athena/software/aeroutil-v1.0/Xfoil.

[20] H.G. Weller, G. R. Tabor, H. Jasak, C. Fureby, A tensorial approach to computational continuum mechanics using object orientated techniques, Computational Physics 12 (6) (1998) 620–631.

[21] OpenFoam, Released via the OpenFOAM Foundation, See http://openfoam.org.

[22] C.M. Rhie, W.L. Chow, A numerical study of the turbulent flow past an isolated airfoil with trailing edge separation, AIAA.J. 21 (1983) 1225–1232.

[23] N. Kolekar and A. Banerjee, Performance characterization and placement of a marine hydrokinetic turbine in a tidal channel under boundary proximity and blockage effects, Applied Energy 148 (2015) 121–133.

[24] C. A. Consul, R. H. J. Willden and S. C. McIntosh, Blockage effects on the hydrodynamic performance of a marine cross-flow turbine, Philosophical Transactions of the Royal Society A 371: 20120299.

[25] H. Sarlak, T. Nishino, L.A. Martnez-Tossas, C. Meneveau and J.N. Sørensen, Assessment of blockage effects on the wake characteristics and power of wind turbines, Renewable Energy 93 (2016) 340–352.